ORGANIC CHEMISTRY FRONTIERS

RESEARCH ARTICLE

View Article Online
View Journal

Cite this: DOI: 10.1039/d5qo00639b

Quinoline-substituted excited-state intramolecular proton transfer fluorophores as stimuli-sensitive dual-state fluorophores†

Timothée Stoerkler,‡[a] Gilles Ulrich,[a] Adèle D. Laurent,[b] Denis Jacquemin *[b,c] and Julien Massue *[a]

Received 13th April 2025,
Accepted 21st July 2025

DOI: 10.1039/d5qo00639b

rsc.li/frontiers-organic

This article describes the synthesis, along with comprehensive photophysical and *ab initio* characterization, of a series of 2-(2′-hydroxyphenyl)benzoxazole (HBO) fluorophores, a family of compounds prone to undergoing an excited-state intramolecular proton transfer (ESIPT) process, functionalized with different positional isomers of quinoline or isoquinoline. We notably show that the position of the nitrogen atom at the azaheterocycle site has a key influence on both the emission profile and the photoluminescence quantum yield in solution. We also demonstrate the proton-sensitive nature of these dyes in solution, where not only does protonation trigger fluorescence enhancement, but it also acts as a transition switch between two excited states, with different emission profiles. HBO-isoquinoline displays very intense fluorescence not only in neutral and protonated dichloromethane solutions in the green-yellow region, but also in the solid state. Moreover, this dye exhibited a record Stokes shift of 11 000 cm^{-1}.

Introduction

Excited-state intramolecular proton transfer (ESIPT) is a four-level photophysical process that can occur in heterocycles possessing a strong intramolecular hydrogen bond in their structure, and it corresponds to an ultrafast internal proton transfer turning a normal species (N*) into its tautomeric (T*) counterpart in the excited state.[1] In the majority of examples, ESIPT involves excited enol (E*) and keto (K*) isomers, respectively, acting as N* and T*, with typical proton donors and acceptors being phenol and nitrogen heterocycles, respectively. A well-studied family is composed of 2-(2′-hydroxyphenylbenzazole) (HBX) dyes, largely owing to their synthetic availability and important modularity.[2]

ESIPT implies a major reorganization of the electronic cloud in the molecular scaffold, eventually leading to a low-lying K* state, responsible for a redshifted K* fluorescence (Fig. 1a). ESIPT is indeed characterized by important Stokes' shifts, in the 8000–10 000 cm^{-1} range, a feature highly beneficial for applications where reabsorption processes and related inner-filter effects hamper the use of fluorescent organic scaffolds presenting a significant overlap between the absorption and emission spectra.[3] Moreover, ESIPT can compete with other processes in the excited state such as proton abstraction, leading, in basic or dissociative media, to highly emissive anionic species (D* state).[4] All these excited-state dynamical processes have nonetheless detrimental effects on the overall performance of fluorescent dyes, as efficient non-radiative pathways tend to decrease the fluorescence intensity of ESIPT dyes in solution; the photoluminescence quantum yields (QYs) of unsubstituted HBX dyes are typically in the 0.01–0.03 range, due to an accessible conical intersection (CI), corresponding to the twisting of the molecule after proton transfer.[5] The access to this CI can be significantly hampered in the solid state, making ESIPT fluorophores attractive solid-state emitters, contrasting with the majority of molecular dyes where aggregative processes open non-radiative channels.[6] ESIPT dyes have therefore been largely used for their solid-state luminescence properties[7] and applied in optoelectronic devices,[8] as laser dyes[9] or embedded in various luminescent displays.[10]

Dual solution–solid emission (DSSE) corresponds to a highly sought-after property of some fluorophores which display intense luminescence both in solution and in the solid state.[11] DSSE has emerged as an attractive area of research, due to the large array of applications targeted by these dyes, in

[a]*Institut de Chimie et Procédés pour l'Energie, l'Environnement et la Santé (ICPEES), UMR CNRS 7515, Equipe Chimie Organique pour la Biologie, les Matériaux et l'Optique (COMBO), 25 Rue Becquerel, 67087 Strasbourg Cedex 02, France. E-mail: massue@unistra.fr*
[b]*Nantes Université, CNRS, CEISAM UMR CNRS 6230, F-44000 Nantes, France. E-mail: Denis.Jacquemin@univ-nantes.fr*
[c]*Institut Universitaire de France (IUF), F-75005 Paris, France*

† Electronic supplementary information (ESI) available: ^{1}H and ^{13}C NMR spectra, details of the computational procedures and methods, and EDD plots for all compounds. See DOI: https://doi.org/10.1039/d5qo00639b

‡ Present address: University of Ottawa, Department of Chemistry, D'Iorio Hall, 10 Marie Curie, Ottawa ON Canada, K1N 6N5

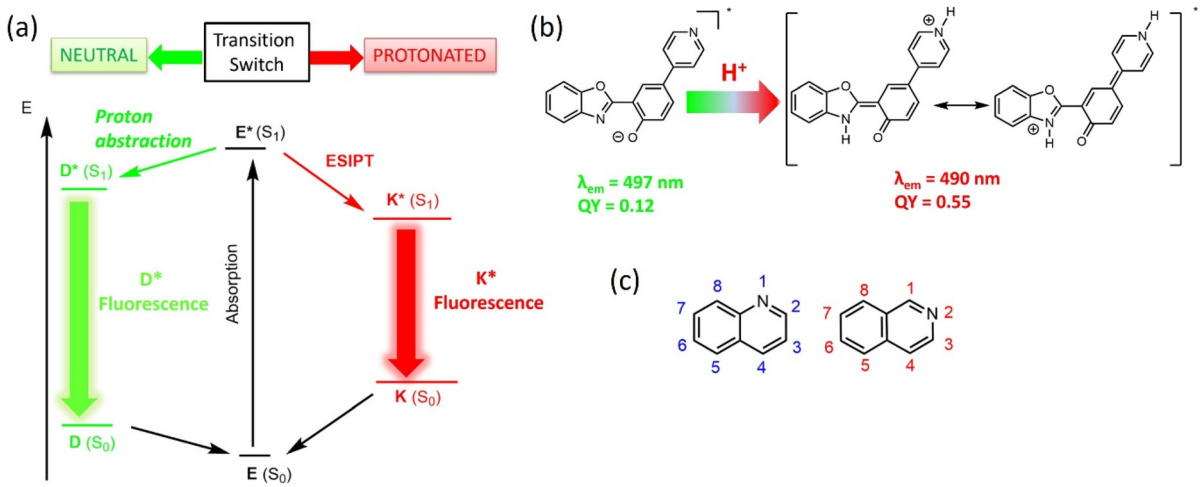

Fig. 1 (a) Jablonski diagram of a transition switch between proton abstraction (deprotonation) and ESIPT upon protonation, (b) HBO-pyridine derivative and its photophysical properties in neutral and protonated media and (c) structures and numbering of quinoline and isoquinoline heterocycles.

the fields of materials science and biology.[12] ESIPT dyes that already exhibit strong emission in the solid state are naturally attractive candidates for DSSE engineering, provided a reduction of non-radiative deactivation processes in solution is obtained.[13] Some solution-emissive ESIPT compounds are known, involving limited access to the CI owing to molecular rigidity enhancement[14] or the insertion of electron-withdrawing substituents onto the molecular scaffold.[15] We[16] and others[17] have detailed another strategy to promote fluorescence intensity in solution, based on the concept of resonance-enhanced emission.[18] A recent example involves a pyridine-substituted 2-(2′-hydroxyphenylbenzoxazole) (HBO) fluorophore. In neutral media, this dye undergoes deprotonation in lieu of ESIPT, thanks to the electron-withdrawing nature of the pyridine ring. An excited anion is formed with a QY of 0.12 (Fig. 1b). When protons are present, a pyridinium is formed, impeding deprotonation and leading to K*, formed by ESIPT, and presenting enhanced electronic delocalization. This merocyanine-type excited species is highly emissive (QY = 0.55) in solution and its excited-state energy level can be fine-tuned by chemical substitution.[19]

One drawback of this pyridine substitution on HBO lies in the emission wavelength observed, in either neutral or protonated media, below 500 nm, which impedes the use of these highly emissive compounds for biological applications, which require emission within the so-called biological window, where the absorption by biological tissues is minimal. One way to redshift the emission wavelength of the resonance-stabilized ESIPT emission would be to substitute pyridine for quinoline or isoquinoline analogs (Fig. 1c). Indeed, increasing the length of the excited merocyanine through longer π-delocalization is expected to stabilize the LUMO, leading to a significant bathochromic shift of the fluorescence wavelength.[20] Notably, a recent example emphasizes that the replacement of a pyridine with a quinoline analog on an imidazole core leads to red shifts of both the absorption and emission wavelengths by up to 150 nm.[21]

In this contribution, we report synthetic efforts to introduce a quinoline ring onto the HBO scaffold, along with a full investigation of the photophysical properties in solution and in the solid state. Moreover, the nature of the observed transitions is rationalized and discussed using first-principles calculations.

Results and discussion

Synthesis

In order to synthesize the target (iso)quinoline-substituted HBO dyes, a strategy similar to that previously used to introduce the pyridine ring was first considered, *i.e.* Pd-catalyzed Suzuki cross-coupling between boronic esters of (iso)quinolines and **HBO-Br**.[19] A series of four (iso)quinolines functionalized with 4,4,5,5-tetramethyl-1,3,2-dioxaborolane (Bpin) was first obtained by halogen–metal exchange with bromo precursors, followed by reaction with an appropriate electrophile to yield compounds **1–4** in 42 to 73% yields (Scheme 1). (Iso)quinolines **1–4** were then engaged in Suzuki couplings with **HBO-Br**, following the previously optimized protocol, *i.e.*, using $Pd(dppf)Cl_2$ as a catalyst, with potassium carbonate as a base in a toluene/ethanol mixture (Scheme 2).

While **HBO-5-quino** was obtained with a good yield of 68%, other quinoline or isoquinoline isomers **HBO-4-quino** and **HBO-6-isoquino** were obtained in only 16 and 17% yields. Moreover, the formation of **HBO-6-quino** was not observed under these coupling conditions. These low yields can be tentatively explained by the poor reactivity of (iso)quinolines **1–4**, whose carbon adjacent to boron features a weak electron density due to the electron-withdrawing nature of the (iso)quinoline group.

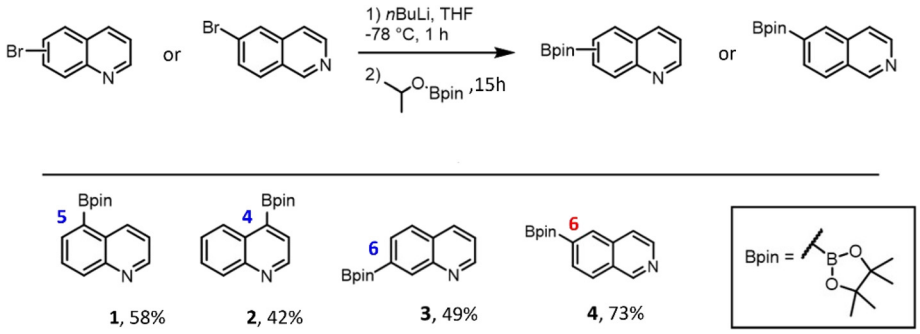

Scheme 1 Synthesis of Bpin-quinolines **1–3** and Bpin-isoquinoline **4**.

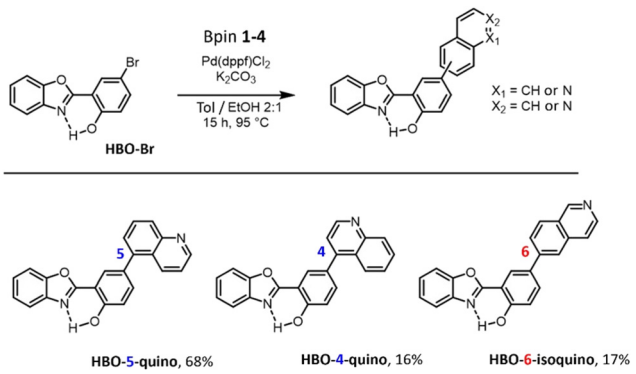

Scheme 2 Synthesis of HBO quinolines and isoquinoline *via* Pd-catalyzed cross-coupling between **HBO-Br** and Bpin derivatives **1–4**.

Reversing the nature of the coupling partners in the Suzuki cross-coupling, *i.e.*, using commercial brominated (iso)quinolines with reported **HBO-Bpin**, under modified coupling conditions ($Pd(dppf)Cl_2$ with potassium phosphate in a toluene/H_2O mixture) led to the access of all desired (iso)quinoline targets in 53 to 78% yields (Scheme 3). The molecular structures of all these compounds were confirmed by ^1H and ^{13}C NMR spectroscopy and HR-MS (Fig. S1–S16†).

Photophysical properties

The photophysical properties of all compounds were studied in both neutral and protonated dichloromethane as well as in the solid state. The photophysical data are compiled in Table 1, while absorption and emission spectra are presented in Fig. 2 and 3. The data and spectra of **HBO-Pyr** were added for comparison.

In neutral dichloromethane, all HBO (iso)quinoline dyes exhibit a low-lying S_0–S_1 absorption band located between 326 and 340 nm with absorption coefficient ε values between 12 800 and 21 500 M^{-1} cm^{-1} (Fig. 2a and b). Interestingly, **HBO-6-isoquino** is the most redshifted in the series (λ_{abs} = 340 nm) with the lowest ε value (ε = 12 800 M^{-1} cm^{-1}). Protonation of the dichloromethane solutions by bubbling HCl_g leads to the formation of the quinolinium analogs of all dyes, which triggers the appearance of a new bathochromically shifted absorption band (λ_{abs} = 344 to 377 nm; ε = 15 to 23 000 M^{-1} cm^{-1}). In a neutral medium, the absorption spectra of all (iso)quinoline dyes are in the same range as that of **HBO-Pyr**,

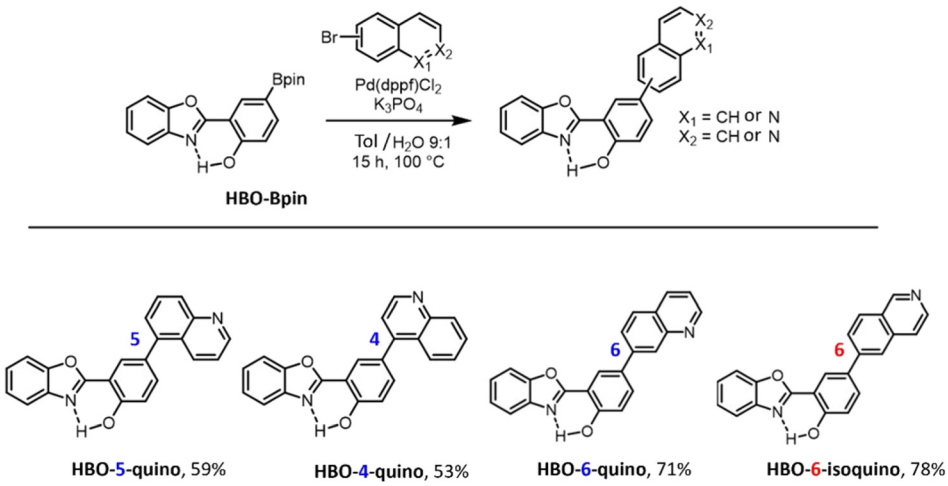

Scheme 3 Synthesis of HBO quinolines and isoquinoline *via* Pd-catalyzed cross-coupling between **HBO-Bpin** and Br-quinolines or isoquinoline.

Table 1 Photophysical data in solution and in the solid state

HBO	Solvent/solid	λ_{abs} [a] (nm)	ε (M^{-1} cm^{-1})	λ_{em} [b] (nm)	Φ_f [c]	Δ_{ss} [d] (cm^{-1})	σ (ns)	K_r [e]	K_{nr} [e]
HBO-Pyr	CH_2Cl_2	332	14 200	497	0.12	10 000	3.4	0.4	0.26
	CH_2Cl_2/H^+	330	29 300	490	0.55	9900	3.5	0.16	0.13
	Solid	330[f]	—	496	0.38	10 100	—	—	—
HBO-4-quino	CH_2Cl_2	326	18 000	504	0.12	10 800	1.5	0.08	0.59
	CH_2Cl_2/H^+	360	15 000	560	0.08	9900	1.7	0.05	0.53
	Solid	364[f]	—	517	0.39	8100	—	—	—
HBO-5-quino	CH_2Cl_2	328	16 800	513	0.04	11 000	0.9	0.05	1.10
	CH_2Cl_2/H^+	333/379	17 000	500/671	0.01	6400	7.7	0.01	0.13
	Solid	367[f]	—	510	0.44	7600	—	—	—
HBO-6-quino	CH_2Cl_2	335	21 500	523	0.12	10 700	1.4	0.09	0.63
	CH_2Cl_2/H^+	341/377	20 000	510/624	0.07	6900	0.9	0.08	1.03
	Solid	371[f]	—	531	0.50	8100	—	—	—
HBO-6-isoquino	CH_2Cl_2	340	12 800	544	0.21	11 000	2.1	0.10	0.38
	CH_2Cl_2/H^+	344	23 000	548	0.79	10 800	3.5	0.22	0.06
	Solid	374[f]	—	525	0.40	7700	—	—	—

[a] Maximum absorption wavelength ($C = 10^{-5}$ M). [b] Maximum emission wavelength recorded at 25 °C ($C = 10^{-6}$ M for solution measurements). [c] Quantum yield in solution, using rhodamine 6G as a reference (λ_{exc} = 488 nm and Φ = 0.88 in ethanol); quantum yield in the solid state, as absolute (calculated with an integration sphere). [d] Stokes shift. [e] k_r (10^8 s^{-1}) and k_{nr} (10^8 s^{-1}) were calculated using $k_r = \Phi_F/\tau$ and $k_{nr} = (1 - \Phi_F)/\tau$, where τ is the lifetime. [f] Excitation wavelength.

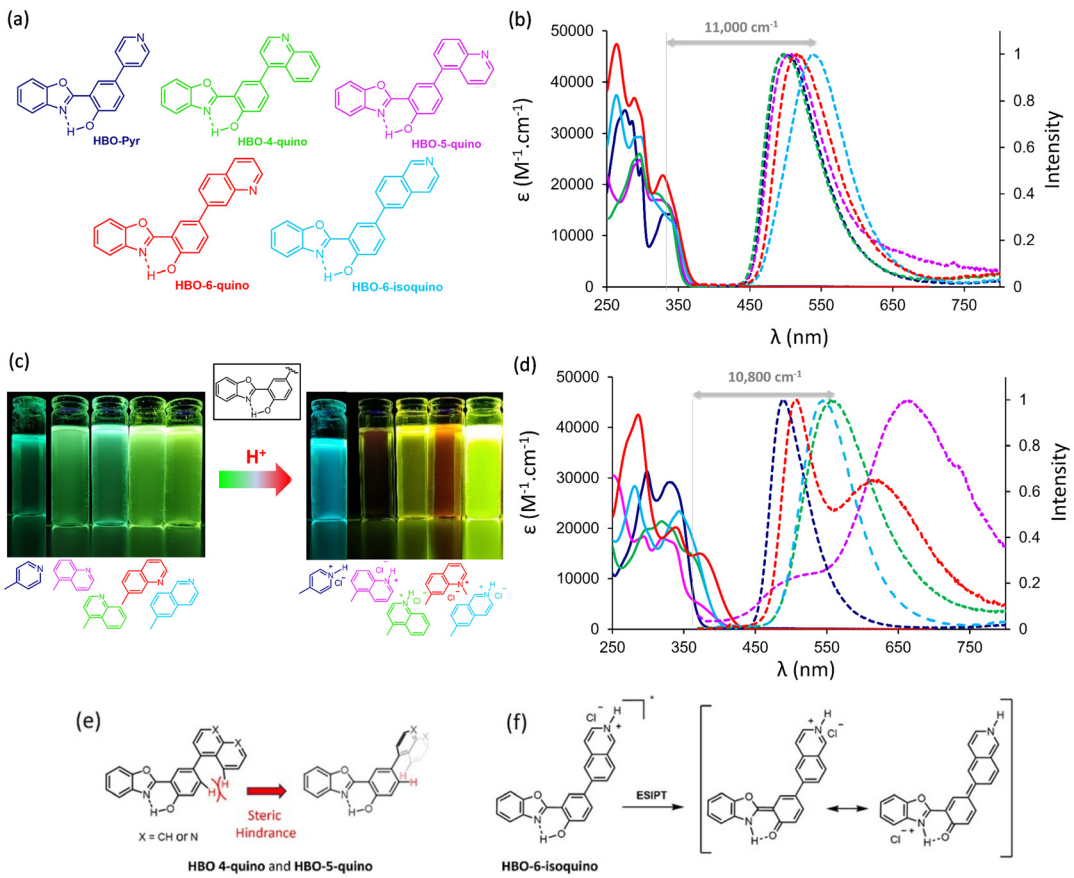

Fig. 2 (a) Molecular structures of **HBO-Pyr**, **HBO-4-quino**, **HBO-5-quino**, **HBO-6-quino** and **HBO-6-isoquino**. Absorption (solid lines) and emission (dotted lines) spectra of **HBO-Pyr** (navy), **HBO-4-quino** (green), **HBO-5-quino** (purple), **HBO-6-quino** (red) and **HBO-6-isoquino** (blue) in (b) neutral and (d) protonated dichloromethane solutions. (c) Photographs in dichloromethane solutions under irradiation (λ_{exc} = 365 nm). (e) Representation of the steric hindrance occurring for **HBO-4-quino** and **HBO-5-quino**. (f) Representation of the resonance-stabilized conformation of **HBO-6-isoquino** in the excited state upon protonation.

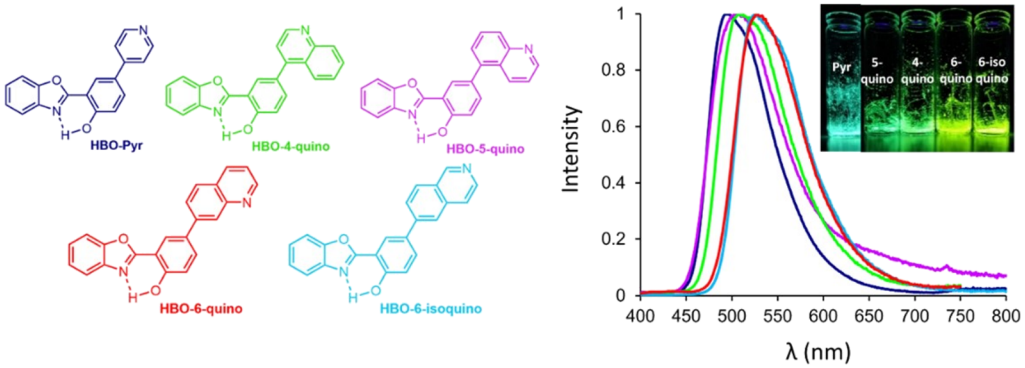

Fig. 3 Emission spectra of **HBO-Pyr** (navy), **HBO-4-quino** (green), **HBO-5-quino** (purple), **HBO-6-quino** (red) and **HBO-6-isoquino** (blue) as powders in the solid state (inset: photographs of all powders under UV irradiation, λ_{exc} = 365 nm).

but after protonation, they all show a redshifted absorption band as compared to the pyridine analogue (Fig. 2c and d).

Photoexcitation in the S_0–S_1 band yields a single intense emission band in neutral dichloromethane solution, observed between 500 and 560 nm with QY values in the 0.04–0.21 range. These emission wavelengths are all redshifted compared to the reference **HBO-Pyr** (λ_{em} = 497 nm and QY = 0.12). **HBO-6-isoquino** is the most redshifted fluorophore of the series, along with the highest QY value (0.21).

It was previously reported that the emission of **HBO-Pyr** in neutral dichloromethane likely arose from an anionic excited species D*, although it was not entirely possible to rule out the possibility of emission from the K* state, as it was uneasy to distinguish between these two transitions.[16,19] This analysis was based on significant changes in its optical profile after protonation and was consistent with the results of *ab initio* calculations. Compared to **HBO-Pyr**, the quinoline analogs show significant changes in their emission profiles in the presence of protons. Notably, upon protonation, the maximum emission wavelengths of **HBO-4-quino** and **HBO-6-isoquino** undergo bathochromic shifts to different extents (λ_{em} = 560 *vs.* 504 nm for **HBO-4-quino** and 548 *vs.* 544 nm for **HBO-6-isoquino** in the protonated *vs.* the neutral state, respectively), underlining the significant influence of the nature of (iso)quinoline positional isomers. Moreover, in their protonated state, while **HBO-4-quino** does not exhibit a drastic change in its fluorescence intensity (QY = 0.08 *vs.* 0.12), **HBO-6-isoquino** displays intense emission (QY = 0.79). In the latter case, the fluorescence band observed can be tentatively attributed to the decay of K*, stabilized by electronic delocalization (*vide infra*). In both cases, these two dyes display very large Stokes shifts, up to 11 000 cm^{-1} (204 nm), which rank them among the organic fluorophores with the largest Stokes shifts, highlighting a major structural reorganization of the excited state.[3a] Upon protonation, **HBO-5-quino** and **HBO-6-quino** show different emission profiles with two distinct bands at 500/671 nm and 510/624 nm, respectively. Their QY values are, however, modest (0.01 and 0.07 for **HBO-5-quino** and **HBO-6-quino**, respectively). In protonated media, the formation of the quinolinium moiety impedes the emission of the anionic excited species D*, suggesting that the emission bands observed could be associated with the decay of E* and its tautomeric counterpart, K*, formed after ESIPT.

One can easily and visually notice in Fig. 2c that only the emission intensity of **HBO-6-isoquino** drastically increases upon protonation of the dichloromethane solution, going from 0.21 to 0.79. We cautiously interpret this significant enhancement of the fluorescence as arising from the resonance stabilization of the excited keto species, formed after ESIPT (Fig. 2f). The π-delocalization in the K* form enables the formation of a quinoidal species, which is likely less prone to the out-of-plane motions leading to a CI structure. For all other positional isomers, it is possible to rationalize the weak fluorescence intensity observed for **HBO-4-quino** and **HBO-5-quino** by the presence of detrimental steric interactions, leading to a rotation or a twist of the quinoline ring, hampering planarity and electronic delocalization and ultimately enhancing non-radiative deactivation (Fig. 2e). In the case of **HBO-6-quino**, the radiative deactivation constant K_r is much lower than that of its **HBO-Pyr** counterpart and *vice versa* for the nonradiative deexcitation constant K_{nr}. This reflects a less stabilized, excited state mesomeric form. This could simply be due to the position of the nitrogen in the azaheterocycle, at the "pseudo *para*" position unfavorable for delocalization.

The optical properties of all (iso)quinoline HBOs were also measured in the solid state as powders (Fig. 3). They all display an intense single emission band ranging from 510 to 531 nm, redshifted with respect to **HBO-Pyr**. The QY values (0.39 to 0.50) are in line with those observed for the pyridine-substituted HBO series.[19]

It is noteworthy that **HBO-6-isoquino** displays very attractive features: intense fluorescence both in dichloromethane solution (λ_{em} = 544 nm and QY = 0.21) and in the solid state as powder (λ_{em} = 525 nm and QY = 0.40) with a very large Stokes shift in both media (11 000 cm^{-1}). Moreover, **HBO-6-isoquino** is very sensitive to protonation stimuli, triggering a transition switch in the presence of protons. The formation of the isoquinolinium moiety indeed translates into a very important enhancement of fluorescence intensity (0.21 to 0.79), with a similarly large Stokes shift.

To further characterize these systems, we used *ab initio* calculations, using the same protocol as the one we recently applied for pyridine-substituted HBO derivatives.[19] This protocol combines TD-DFT for the structures and a post-HF approach (CC2) for the energies. The electron density difference (EDD) plots are presented in section S3.2,† for the absorption of both neutral and protonated dyes. For the neutral compound, these plots show a classical topology for ESIPT dyes, *i.e.*, a hydroxyl group losing density upon excitation, indicating an increase of acidity in the excited state, a configuration obviously favorable for proton transfer. The topology changes drastically after protonation, since the lowest excited state becomes a clear charge transfer state, with the pyridinium/isoquinolinium acting as an electron acceptor and the phenol as an electron donor. Such trends are consistent with our previous works.[16,19] The topologies of the EDDs are not much affected by the nature of the substituent in the investigated series.

Table 2 lists the key results of the theoretical simulations. It should be recalled that vertical transition values are not equivalent to observed λ_{max} (or λ_{em}), which is why we mainly focus on the trends and orders of magnitude in the following discussion. For absorption, one can note that we compute vertical transition energies that are similar within the series for the neutral forms, whereas protonation induces bathochromic shifts that are significantly larger for the (iso)quinolinium than the pyridinium dyes. All these trends are consistent with experimental findings (*vide supra*).

Let us now turn towards fluorescence in neutral dichloromethane. For **HBO-Pyr**, theory provides a large driving force of −0.24 eV for the ESIPT process together with an emission wavelength of 360 nm for the E* form, clearly not compatible with experimental outcomes (emission at 497 nm with a very large Stokes shift). Therefore, consistent with previous studies,[16,19] the observed emission would likely arise from the D* transition, although K* cannot be ruled out. Note that these spectral variations are accompanied by significant structural changes. In **HBO-Pyr**, the dihedral angle between the pyridinium and the phenol is 36° in the ground electronic E state, and it decreases to 27°, indicating stronger conjugation in the excited state (K*). Protonation decreases these values to 31° (E ground state) and 19° (K* excited state), which is consistent with the topology of the EDD, indicating a strong interaction between the two rings when the pyridinium is formed.

For all the other dyes, theory also predicts similarly large free energy differences between the enol and keto forms, allowing the exclusion of the presence of E* emission in all cases. Interestingly, theory predicts the anionic (D*) emission to be redshifted as compared to its K* counterpart in all (iso)quinoline derivatives, whereas the reverse was found in **HBO-Pyr**. For **HBO-5-quino**, the D* fluorescence is predicted at 600 nm, redshifted by more than 125 nm compared to **HBO-Pyr**, a trend that is not seen experimentally (Fig. 2b). Therefore, we can conclude that the fluorescence of **HBO-5-quino** is a pure K* one. The same holds for both **HBO-4-quino** and **HBO-6-quino**, which exhibit fluorescence, respectively, blueshifted and redshifted by *ca.* 10 nm as compared to **HBO-5-quino** experimentally (Table 1). This trend nicely fits the computed K* fluorescence wavelengths, but would be rather incompatible with D* fluorescence. Finally, we cannot definitively attribute the observed emission of **HBO-6-isoquino** (at 544 nm) to the D* or K* forms, although relative comparisons with the other compounds tend to hint at D* fluorescence.

Of course, the structure of the dye influences its geometry. For instance, in the ground E state (K* form) **HBO-5-quino** shows a dihedral angle of 53° (43°) between the quinoline and the phenol, due to the obvious steric clash appearing between the two cycles in that compound. In contrast, in **HBO-6-isoquino**, this angle amounts to 38° (21°), since the configuration allows for improved coplanarity.

In the presence of protons, the D* fluorescence cannot be observed. In this context, for **HBO-Pyr**, it is clear that the experimental fluorescence corresponds to the K* form since the computed ESIPT driving force remains large (−0.20 eV), and only the computed K* emission produces a Stokes shift comparable with the measurements. In both **HBO-5-quino** and **HBO-6-quino**, two bands are observed experimentally corresponding to a dual E*/K* emission. We note that in these two

Table 2 Computed vertical transition wavelengths (all in nm) for absorption and emission, as well as computed Stokes shifts (in cm^{-1}) as compared to E. The rightmost column contains the difference of free energies between the keto and enol tautomers in their excited state (in eV, a negative value indicating a more stable keto form). All wavelengths were determined with CC2 corrections, as explained in section S3.1,† whereas the relative free energies were obtained from the TD-DFT analytic frequency calculations. All data were computed in dichloromethane using the so-called cLR^2 solvation model

HBO	Form	$\lambda_{vert\text{-}abs}$ (E) (nm)	$\lambda_{vert\text{-}fl}$ (E*) (nm)	$\lambda_{vert\text{-}fl}$ (K*) (nm)	$\lambda_{vert\text{-}fl}$ (D*) (nm)	Δ_{SS} (E*) (cm^{-1})	Δ_{SS} (K*) (cm^{-1})	Δ_{SS} (D*) (cm^{-1})	ΔG (K*–E*) (eV)
HBO-Pyr	Neutral	309	360	467	450	4584	10 949	10 140	−0.24
	Protonated	353	414	500	—	4174	8328		−0.20
HBO-4-quino	Neutral	309	360	466	529	4584	10 903	13 459	−0.23
	Protonated	393	480	637	—	4611	9746		−0.11
HBO-5-quino	Neutral	312	367	473	600	4803	10 910	15 384	−0.21
	Protonated	390	588	859	—	8634	14 000		−0.01
HBO-6-quino	Neutral	316	373	487	532	4835	11 112	12 848	−0.24
	Protonated	391	514	663	–	6120	10 492		−0.07
HBO-6-isoquino	Neutral	316	375	486	507	4978	11 069	11 912	−0.23
	Protonated	368	496	701	—	7013	12 908		−0.04

compounds, the ESIPT driving force is strongly reduced after protonation, leading to small negative ΔG of −0.01 and −0.07 eV, indicating that the K* form is only slightly more stable than its E* counterpart, which fits the presence of dual emission.[22] Obviously for the former compound, theory strongly overestimates the emission wavelengths of the two forms, yet errors of *ca.* 0.4 eV remain, which are large but not impossible at the selected level of theory. The observed emission in CH_2Cl_2/H^+ **HBO-4-quino** is in between the two bands observed for both **HBO-5-quino** and **HBO-6-quino**, which clearly points at K* emission. We note that the driving force for ESIPT in (protonated) **HBO-4-quino** is also larger than those in the other two compounds, consistent with this assignment. Finally, for protonated **HBO-6-isoquino**, the experimental emission wavelength remains mostly unchanged as compared to the neutral form and, according to calculations, this would better fit a computed E* emission, with a large Stokes shift explained by a strong CT character. However, a K* transition, characterized by a resonant quinoidal structure, would be closer to what was evidenced for the pyridine analog, **HBO-pyr**, and cannot be ruled out in our opinion.

Conclusions

In conclusion, the synthesis, along with full photophysical characterization and first-principles calculations, of a series of HBO fluorophores, functionalized with different aza-heterocycles, namely quinoline or isoquinoline, is presented. We demonstrate that the nature of the functionalization is a key parameter to regulate the photophysical properties (emission wavelength and quantum yield). All dyes reported herein are highly sensitive to the presence of protons where protonation acts as a transition switch between two excited states. One compound, HBO-isoquinoline, stands out in the series with a very intense fluorescence in neutral and protonated dichloromethane solutions in the green-yellow region and in the solid state. A record Stokes shift of 11 000 cm^{-1} was observed for this dye, paving the way for its use in bioimaging applications. Work along these lines is currently underway.

Experimental section

HBO-Br and **HBO-Bpin** are reported in the literature.[19]

General procedure for the synthesis of Bpin-quinolines 1–3 and isoquinoline 4

Bromo-quinolines or isoquinoline were dissolved in anhydrous THF (0.1 M), before *n*-BuLi (1.6 M, 1.2 eq.) was added dropwise at −78 °C. The resulting solution was stirred for 1 hour at −78 °C, before 2-isopropoxy-4,4,5,5-tetramethyl-1,3,2-dioxaborolane (1.5 eq.) was added dropwise. The reaction mixture was stirred at −78 °C for 1 hour, warmed up to room temperature and further stirred overnight. A saturated solution of NH_4Cl was then added to quench the reaction and the aqueous phase was extracted with Et_2O three times. The combined organic layers were washed with brine and dried on $MgSO_4$ before being concentrated *in vacuo*. The crude products were purified with silica gel chromatography eluting with petroleum ether/CH_2Cl_2 to afford Bpin-quinolines **1–3** and isoquinoline **4**, as white to yellow solids.

Quinoline 1. 58%. White solid. ^{1}H NMR (500 MHz, $CDCl_3$) δ 9.11 (dd, ^3J = 8.5, ^4J = 1.7 Hz, 1H), 8.91 (dd, ^3J = 4.2, ^4J = 1.7 Hz, 1H), 8.19 (dd, ^3J = 8.5, ^4J = 1.3 Hz, 1H), 8.14 (dd, ^3J = 6.8, ^4J = 1.3 Hz, 1H), 7.71 (dd, ^3J = 8.5, ^3J = 6.8 Hz, 1H), 7.43 (dd, ^3J = 8.5, ^3J = 4.2 Hz, 1H), 1.42 (s, 12H). ^{13}C{^{1}H} NMR (126 MHz, $CDCl_3$) δ = 150.2, 148.2, 136.9, 136.3, 133.1, 132.2, 128.7, 121.5, 84.1, 25.1. HR-MS (ESI-TOF) *m*/*z*: [M + H^+] calc. for $C_{15}H_{19}BNO_2$: 256.1503, found: 256.1497.

Quinoline 2. 42%. White solid. ^{1}H NMR (500 MHz, $CDCl_3$) δ 8.91 (d, ^3J = 4.1 Hz, 1H), 8.64 (dd, ^3J = 8.4, ^4J = 1.5 Hz, 1H), 8.10 (dd, ^3J = 8.5, ^4J = 1.5 Hz, 1H), 7.85 (d, ^3J = 4.1 Hz, 1H), 7.70 (ddd, ^3J = 8.4, ^3J = 6.8, ^4J = 1.5 Hz, 1H), 7.57 (ddd, ^3J = 8.3, ^3J = 6.8, ^4J = 1.5 Hz, 1H), 1.42 (s, 12H). ^{13}C{^{1}H} NMR (126 MHz, $CDCl_3$) δ = 149.6, 148.0, 131.2, 129.8, 129.1, 128.8, 128.5, 126.9, 84.6, 25.1. HR-MS (ESI-TOF) *m*/*z*: [M + H^+] calc. for $C_{15}H_{19}BNO_2$: 256.1503, found: 256.1496.

Quinoline 3. 49%. Yellow solid. ^{1}H NMR (400 MHz, $CDCl_3$) δ 8.93 (dd, ^3J = 4.2, ^4J = 1.8 Hz, 1H), 8.60 (s, 1H), 8.14 (ddd, ^3J = 8.3, ^4J = 1.9, ^4J = 1.0 Hz, 1H), 7.90 (dd, ^3J = 8.1, ^4J = 1.0 Hz, 1H), 7.80 (d, ^3J = 8.1 Hz, 1H), 7.41 (dd, ^3J = 8.3, ^3J = 4.2 Hz, 1H), 1.39 (s, 13H). ^{13}C{^{1}H} NMR (101 MHz, $CDCl_3$) δ = 150.6, 137.4, 136.0, 131.3, 130.1, 127.0, 121.9, 84.3, 25.0. HR-MS (ESI-TOF) *m*/*z*: [M + H^+] calc. for $C_{15}H_{19}BNO_2$: 256.1503, found: 256.1509.

Isoquinoline 4. 73%. White solid. ^{1}H NMR (400 MHz, $CDCl_3$) δ 9.26 (s, 1H), 8.53 (d, ^3J = 5.7 Hz, 1H), 8.34 (s, 1H), 8.03–7.91 (m, 2H), 7.67 (d, ^3J = 5.7 Hz, 1H), 1.40 (s, 12H). ^{13}C{^{1}H} NMR (101 MHz, $CDCl_3$) δ = 152.6, 143.2, 135.2, 134.6, 132.0, 130.0, 126.6, 121.1, 84.5, 25.1. HR-MS (ESI-TOF) *m*/*z*: [M + H^+] calc. for $C_{15}H_{19}BNO_2$: 256.1503, found: 256.1513.

General procedure for the synthesis of HBO-4-quino, HBO-5-quino, HBO-6-quino and HBO-6-isoquino

In a Schlenk tube, 4-, 5-, or 6-bromoquinoline or 6-isoquinoline, **HBO-Bpin** (1.2 eq.), and tripotassium phosphate (4 eq.) were dissolved in a mixture of toluene/H_2O (9/1, v/v, 0.05 M). The resulting suspension was degassed with argon before the addition of $PdCl_2$(dppf) (5% mol) and further stirred at 100 °C using an oil bath for 15 h. The crude solution was then quenched with a solution of saturated NH_4Cl and extracted with ethyl acetate three times. The organic phases were combined, washed with brine, dried over $MgSO_4$ and concentrated *in vacuo*. The crude mixture was purified by silica gel chromatography with CH_2Cl_2/ethanol (98 : 2) to afford **HBO-4-quino**, **HBO-5-quino**, **HBO-6-quino** and **HBO-6-isoquino**, as white to yellow powders.

HBO-4-quino. 53%. Yellow solid. ^{1}H NMR (400 MHz, $CDCl_3$) δ 11.69 (s, 1H), 8.97 (d, ^3J = 4.4 Hz, 1H), 8.24–8.17 (m, 2H), 8.00 (d, ^3J = 8.5 Hz, 1H), 7.82–7.68 (m, 2H), 7.64–7.51 (m, 3H), 7.46–7.35 (m, 3H), 7.29 (d, ^3J = 8.5 Hz, 1H). ^{13}C{^{1}H} NMR (101 MHz, $CDCl_3$) δ = 162.5, 159.1, 150.2, 149.3, 148.9, 147.5, 140.0, 134.8, 130.1, 129.6, 129.5, 128.2, 127.0, 125.8, 125.8,

125.4, 121.5, 119.5, 118.0, 111.0, 110.9. HR-MS (ESI-TOF) *m*/*z*: [M + H$^+$] calc. for $C_{22}H_{15}N_2O_2$: 339.1128, found: 339.1124.

HBO-5-quino. 59%. Yellow solid. ^{1}H NMR (500 MHz, $CDCl_3$) δ 11.63 (s, 1H), 8.96 (dd, ^3J = 4.1, ^4J = 1.7 Hz, 1H), 8.30 (d, ^3J = 8.7 Hz, 1H), 8.21–8.12 (m, 2H), 7.85–7.74 (m, 2H), 7.62–7.51 (m, 3H), 7.47–7.34 (m, 3H), 7.28 (d, ^3J = 8.5 Hz, 1H). ^{13}C{^{1}H} NMR (126 MHz, $CDCl_3$) δ = 162.8, 158.5, 150.4, 149.3, 140.1, 139.5, 135.3, 134.4, 131.0, 129.2, 128.5, 128.2, 128.0, 127.8, 127.6, 127.0, 125.8, 125.3, 121.4, 119.5, 117.8, 110.9. HR-MS (ESI-TOF) *m*/*z*: [M + H$^+$] calc. for $C_{22}H_{15}N_2O_2$: 339.1128, found: 339.1123.

HBO-6-quino. 71%. Yellow solid. ^{1}H NMR (400 MHz, $CDCl_3$) δ 11.59 (s, 1H), 8.97 (s, 1H), 8.47 (d, ^4J = 2.3 Hz, 1H), 8.39 (s, 1H), 8.19 (d, ^3J = 8.2 Hz, 1H), 7.92 (d, ^3J = 8.5 Hz, 1H), 7.90–7.85 (m, 2H), 7.82–7.72 (m, 1H), 7.70–7.61 (m, 1H), 7.47–7.37 (m, 3H), 7.28 (d, ^4J = 2.2 Hz, 1H). ^{13}C{^{1}H} NMR (101 MHz, $CDCl_3$) δ = 162.8, 158.8, 151.1, 149.3, 148.8, 141.0, 140.1, 135.9, 132.5, 131.9, 128.5, 127.4, 126.6, 126.0, 125.8, 125.7, 125.3, 121.1, 119.5, 118.3, 111.2, 110.9. HR-MS (ESI-TOF) *m*/*z*: [M + H$^+$] calc. for $C_{22}H_{15}N_2O_2$: 339.1128, found: 339.1125.

HBO-6-isoquino. 78%. Yellow solid. ^{1}H NMR (400 MHz, $CDCl_3$) δ 11.64 (s, 1H), 9.29 (s, 1H), 8.57 (d, ^3J = 5.8 Hz, 1H), 8.39 (d, ^4J = 2.3 Hz, 1H), 8.07 (d, ^3J = 8.5 Hz, 1H), 8.04 (s, 1H), 7.92 (dd, ^3J = 8.5, ^4J = 1.8 Hz, 1H), 7.82 (dd, ^3J = 8.5, ^4J = 2.4 Hz, 1H), 7.80–7.75 (m, 1H), 7.73 (d, ^3J = 5.7 Hz, 1H), 7.70–7.63 (m, 1H), 7.46–7.39 (m, 2H), 7.27 (d, ^3J = 8.7 Hz, 1H). ^{13}C{^{1}H} NMR (101 MHz, $CDCl_3$) δ = 162.7, 159.0, 152.4, 149.3, 143.7, 142.0, 140.1, 136.4, 132.8, 131.9, 128.5, 127.8, 126.8, 126.1, 125.8, 125.4, 123.7, 120.8, 119.6, 118.4, 111.2, 110.9. HR-MS (ESI-TOF) *m*/*z*: [M + H$^+$] calc. for $C_{22}H_{15}N2O_2$: 339.1128, found: 339.1125.

Conflicts of interest

There are no conflicts to declare.

Data availability

The data supporting this article have been included as part of the ESI.†

Acknowledgements

The authors thank the CNRS for financial support. T. S. acknowledges the University of Strasbourg (ED 222) for a doctoral allocation. This research used resources of the GLiCID Computing Facility (Ligerien Group for Intensive Distributed Computing, **https://doi.org/10.60487/glicid**, Pays de la Loire, France).

References

1 (*a*) J. Zhao, S. Ji, Y. Chen, H. Guo and P. Yang, Excited state intramolecular proton transfer (ESIPT): from principal photophysics to the development of new chromophores and applications in fluorescent molecular probes and luminescent materials, *Phys. Chem. Chem. Phys.*, 2012, **14**, 8803–8817; (*b*) J. Massue, D. Jacquemin and G. Ulrich, Molecular Engineering of Excited-state Intramolecular Proton Transfer (ESIPT) Dual and Triple Emitters, *Chem. Lett.*, 2018, **47**(9), 1083–1089; (*c*) A. C. Sedgwick, L. Wu, H.-H. Han, S. D. Bull, X.-P. He, T. D. James, J. L. Sessler, B. Z. Tang, H. Tian and J. Yoon, Excited-state intramolecular proton-transfer (ESIPT) based fluorescence sensors and imaging agents, *Chem. Soc. Rev.*, 2018, **47**, 8842–8880.

2 (*a*) T. Stoerkler, G. Ulrich, P. Retailleau, A. D. Laurent, D. Jacquemin and J. Massue, Experimental and theoretical comprehension of ESIPT fluorophores based on a 2-(2′-hydroxyphenyl)-3,3′-dimethylindole (HDMI) scaffold, *Chem. Sci.*, 2024, **15**, 7206–7218; (*b*) Y. Chen, Y. Fang, H. Gu, J. Qiang, H. Li, J. Fan, J. Cao, F. Wang, S. Lu and X. Chen, Color-Tunable and ESIPT-Inspired Solid Fluorophores Based on Benzothiazole Derivatives: Aggregation-Induced Emission, Strong Solvatochromic Effect, and White Light Emission, *ACS Appl. Mater. Interfaces*, 2020, **12**(49), 55094–55106; (*c*) V. R. Mishra, C. W. Ghanavatkar and N. Sekar, Towards NIR-Active Hydroxybenzazole (HBX)-Based ESIPT Motifs: A Recent Research Trend, *ChemistrySelect*, 2020, **5**, 2103–2113.

3 (*a*) H. Liu, G. Jiang, G. Ke, T.-B. Ren and L. Yuan, Organic Fluorophores with Large Stokes Shift for Bioimaging and Biosensing, *ChemPhotoChem*, 2024, **8**, e202300277; (*b*) I. Saridakis, M. Riomet, O. J. V. Belleza, G. Coussanes, N. K. Singer, N. Kastner, Y. Xiao, E. Smith, V. Tona, A. de la Torre, E. F. Lopes, P. A. Sánchez-Murcia, L. González, H. H. Sitte and N. Maulide, PyrAtes: Modular Organic Salts with Large Stokes Shifts for Fluorescence Microscopy, *Angew. Chem., Int. Ed.*, 2024, **63**, e202318127; (*c*) H. Chen, L. Liu, K. Qian, H. Liu, Z. Wang, F. Gao, C. Qu, W. Dai, D. Lin, K. Chen, H. Liu and Z. Cheng, Bioinspired large Stokes shift small molecular dyes for biomedical fluorescence imaging, *Sci. Adv.*, 2022, **8**, eabo3289.

4 (*a*) M. Munch, M. Curtil, P. M. Vérité, D. Jacquemin, J. Massue and G. Ulrich, Ethynyl-Tolyl Extended 2-(2′-Hydroxyphenyl)benzoxazole Dyes: Solution and Solid-state Excited-State Intramolecular Proton Transfer (ESIPT) Emitters, *Eur. J. Org. Chem.*, 2019, 1134–1144; (*b*) K.-I. Sakai, T. Ishikawa and T. Akutagawa, A blue-white-yellow color-tunable excited state intramolecular proton transfer (ESIPT) fluorophore: sensitivity to polar–nonpolar solvent ratios, *J. Mater. Chem. C*, 2013, **1**(47), 7866–7871.

5 T. Stoerkler, T. Pariat, A. D. Laurent, D. Jacquemin, G. Ulrich and J. Massue, Sterically Hindered 2-(2′-Hydroxyphenyl)benzoxazole (HBO) Emitters: Synthesis, Spectroscopic Studies, and Theoretical Calculations, *Eur. J. Org. Chem.*, 2022, e202200661.

6 V. S. Padalkar and S. Seki, Excited-state intramolecular proton-transfer (ESIPT)-inspired solid state emitters, *Chem. Soc. Rev.*, 2016, **45**, 169–202.

7 (*a*) P. Gayathri, M. Pannipara, A. G. Al-Sehemi and S. P. Anthony, Recent advances in excited state intramolecular proton transfer mechanism-based solid state fluorescent materials and stimuli-responsive fluorescence switching, *CrystEngComm*, 2021, **23**, 3771–3789; (*b*) L. Chen, P.-Y. Fu, H.-P. Wang and M. Pan, Excited-State Intramolecular Proton Transfer (ESIPT) for Optical Sensing in Solid State, *Adv. Opt. Mater.*, 2021, **9**(23), 2001952.

8 (*a*) J. E. Kwon and S. Y. Park, Advanced Organic Optoelectronic Materials: Harnessing Excited-State Intramolecular Proton Transfer (ESIPT) Process, *Adv. Mater.*, 2011, **23**(32), 3615–3642; (*b*) M. Mamada, Activated Delayed Fluorescence from an Excited-State Intramolecular Proton Transfer System, *ACS Cent. Sci.*, 2017, **3**(7), 769.

9 C.-C. Yan, X.-D. Wang and L.-S. Liao, Organic Lasers Harnessing Excited State Intramolecular Proton Transfer Process, *ACS Photonics*, 2020, **7**(6), 1355–1366.

10 Y. Zhang, H. Yang, H. Ma, G. Bian, Q. Zang, J. Sun, C. Zhang, Z. An and W.-Y. Wang, Excitation Wavelength Dependent Fluorescence of an ESIPT Triazole Derivative for Amine Sensing and Anti-Counterfeiting Applications, *Angew. Chem., Int. Ed.*, 2019, **58**, 8773–8778.

11 (*a*) H. Wu, Z. Chen, W. Chi, A. K. Bindra, L. Gu, C. Qian, B. Wu, B. Yue, G. Liu, G. Yang, L. Zhu and Y. Zhao, Structural Engineering of Luminogens with High Emission Efficiency Both in Solution and in the Solid State, *Angew. Chem., Int. Ed.*, 2019, **58**, 11419–11423; (*b*) T. Stoerkler, G. Ulrich, A. D. Laurent, D. Jacquemin and J. Massue, Interplay between Dual-State and Aggregation-Induced Emission with ESIPT Scaffolds Containing Triphenylamine Substituents: Experimental and Theoretical Studies, *J. Org. Chem.*, 2023, **88**, 9225–9236.

12 (*a*) J. L. Belmonte-Vazquez, Y. A. Amador-Sanchez, L. A. Rodriguez-Cortes and B. Rodriguez-Molina, Dual-State Emission (DSE) in Organic Fluorophores: Design and Applications, *Chem. Mater.*, 2021, **33**, 7160–7184; (*b*) A. Huber, J. Dubbert, T. D. Scherz and J. Voskuhl, Design Concepts for Solution and Solid-State Emitters – A Modern Viewpoint on Classical and Non-Classical Approaches, *Chem. – Eur. J.*, 2023, **29**, e202202481.

13 (*a*) M. Durko-Maciag, G. Ulrich, D. Jacquemin, J. Mysliwiec and J. Massue, Solid-state emitters presenting a modular excited-state proton transfer (ESIPT) process: recent advances in dual-state emission and lasing applications, *Phys. Chem. Chem. Phys.*, 2023, **25**, 15085–15098; (*b*) T. Stoerkler, T. Pariat, A. D. Laurent, D. Jacquemin, G. Ulrich and J. Massue, Excited-State Intramolecular Proton Transfer Dyes with Dual-State Emission Properties: Concept, Examples and Applications, *Molecules*, 2022, **27**, 2443.

14 (*a*) K. Skonieczny, J. Yoo, J. M. Larsen, E. M. Espinoza, M. Barbasiewicz, V. I. Vullev, C.-H. Lee and D. T. Gryko, How To Reach Intense Luminescence for Compounds Capable of Excited-State Intramolecular Proton Transfer?, *Chem. – Eur. J.*, 2016, **22**, 7485–7496; (*b*) J. Massue, A. Felouat, M. Curtil, P. M. Vérité, D. Jacquemin and G. Ulrich, Solution and solid-state Excited-State Intramolecular Proton Transfer (ESIPT) emitters incorporating Bis-triethyl-or triphenylsilylethynyl units, *Dyes Pigm.*, 2019, **160**, 915–922; (*c*) T. Pariat, M. Munch, M. Durko-Maciag, J. Mysliwiec, P. Retailleau, P. M. Vérité, D. Jacquemin, J. Massue and G. Ulrich, Impact of Heteroatom Substitution on Dual-State Emissive Rigidified 2-(2′-hydroxyphenyl)benzazole Dyes: Towards Ultra-Bright ESIPT Fluorophores, *Chem. – Eur. J.*, 2021, **27**(10), 3483–3495.

15 (*a*) D. Göbel, D. Duvinage, T. Stauch and B. J. Nachtsheim, Nitrile-substituted 2-(oxazolinyl)-phenols: minimalistic excited-state intramolecular proton transfer (ESIPT)-based fluorophores, *J. Mater. Chem. C*, 2020, **8**, 9213–9225; (*b*) D. Göbel, P. Rusch, D. Duvinage, T. Stauch, N.-C. Bigall and B. J. Nachtsheim, Substitution Effect on 2-(Oxazolinyl)-phenols and 1,2,5-Chalcogenadiazole-Annulated Derivatives: Emission-Color-Tunable, Minimalistic Excited-State Intramolecular Proton Transfer (ESIPT)-Based Luminophores, *J. Org. Chem.*, 2021, **86**, 14333–14355.

16 (*a*) T. Pariat, T. Stoerkler, C. Diguet, A. D. Laurent, D. Jacquemin, G. Ulrich and J. Massue, Dual Solution-/Solid-State Emissive Excited-State Intramolecular Proton Transfer (ESIPT) Dyes: A Combined Experimental and Theoretical Approach, *J. Org. Chem.*, 2021, **86**, 17606–17619; (*b*) T. Stoerkler, A. D. Laurent, G. Ulrich, D. Jacquemin and J. Massue, Influence of ethynyl extension on the dual-state emission properties of pyridinium-substituted ESIPT fluorophores, *Dyes Pigm.*, 2022, **208**, 110872.

17 X. Yang, Z. Yang, H. Li, X. Yang and Y. Zhang, Control over rotary motion and multicolour switching in 3-hydroxyphthalimide fluorophores: An interplay between AIE and ESIPT, *Dyes Pigm.*, 2023, **214**, 111215.

18 X. Liu, F. Zhao, B. Chen, Y. Huang, L. Xu, E. Li, L. Tan and H. Zhang, Resonance-Enhanced Emission Effects toward Dual-State Emissive Bright Red and Near-Infrared Emitters, *Chem. – Eur. J.*, 2023, **29**(34), e202300381.

19 (*a*) T. Stoerkler, G. Ulrich, P. Retailleau, S. Achelle, A. D. Laurent, D. Jacquemin and J. Massue, Stimuli-Induced Fluorescence Switching in Azine-Containing Fluorophores Displaying Resonance-Stabilized ESIPT Emission, *Chem. – Eur. J.*, 2024, **30**(56), e202402448; (*b*) T. Stoerkler, A. Nicolas, J. El Aghar, G. Ulrich, A. D. Laurent, D. Jacquemin and J. Massue, Red–Shifting ESIPT Fluorescence by Site–Specific Functionalization in 2–(2′–hydroxyphenyl)benzazole Derivatives, *ChemPhotoChem*, 2024, **8**(10), e202400079.

20 H. Kobayashi, M. Ogawa, R. Alford, P. L. Choyke and Y. Urano, New Strategies for Fluorescent Probe Design in Medical Diagnostic Imaging, *Chem. Rev.*, 2010, **110**, 2620–2640.

21 Y. Xiao, K. Zheng, N. Zhang, Y. Wang, J. Yan, D. Wang and X. Liu, Facile Synthesis of Tetraphenylethene (TPE)-Based Fluorophores Derived by π-Extended Systems: Opposite Mechanofluorochromism, Anti-Counterfeiting and Bioimaging, *Chem. – Eur. J.*, 2023, **29**, e202203772.

22 C. Azarias, S. Budzák, A. D. Laurent, G. Ulrich and D. Jacquemin, Tuning ESIPT fluorophores into dual emitters, *Chem. Sci.*, 2016, **120**, 3763–3774.